National Science Foundation

University of California at San Diego NHERI Natural Hazards Engineering Research Infrastructure

UC San Diego JACOBS SCHOOL OF ENGINEERING Structural Engineering

Soil-Structure Interaction Issues

Scott J. Brandenberg, UCLA

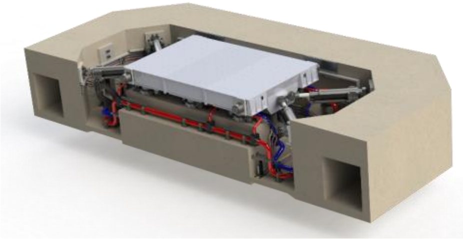

NHERI@UC San Diego User Training Workshop

December 15-16, 2022
University of California, San Diego

Motivation

- Soil-structure interaction (SSI) is coupling of structural and soil responses
- SSI can be modeled using techniques ranging from simple (e.g., "springs" attached to the base of structural elements) to complex (e.g., 3D nonlinear effective stress analysis combining soil and structural elements).
- However, it is very often ignored. Why?

Motivation

- SSI requires effective communication between structural and geotechnical engineers.

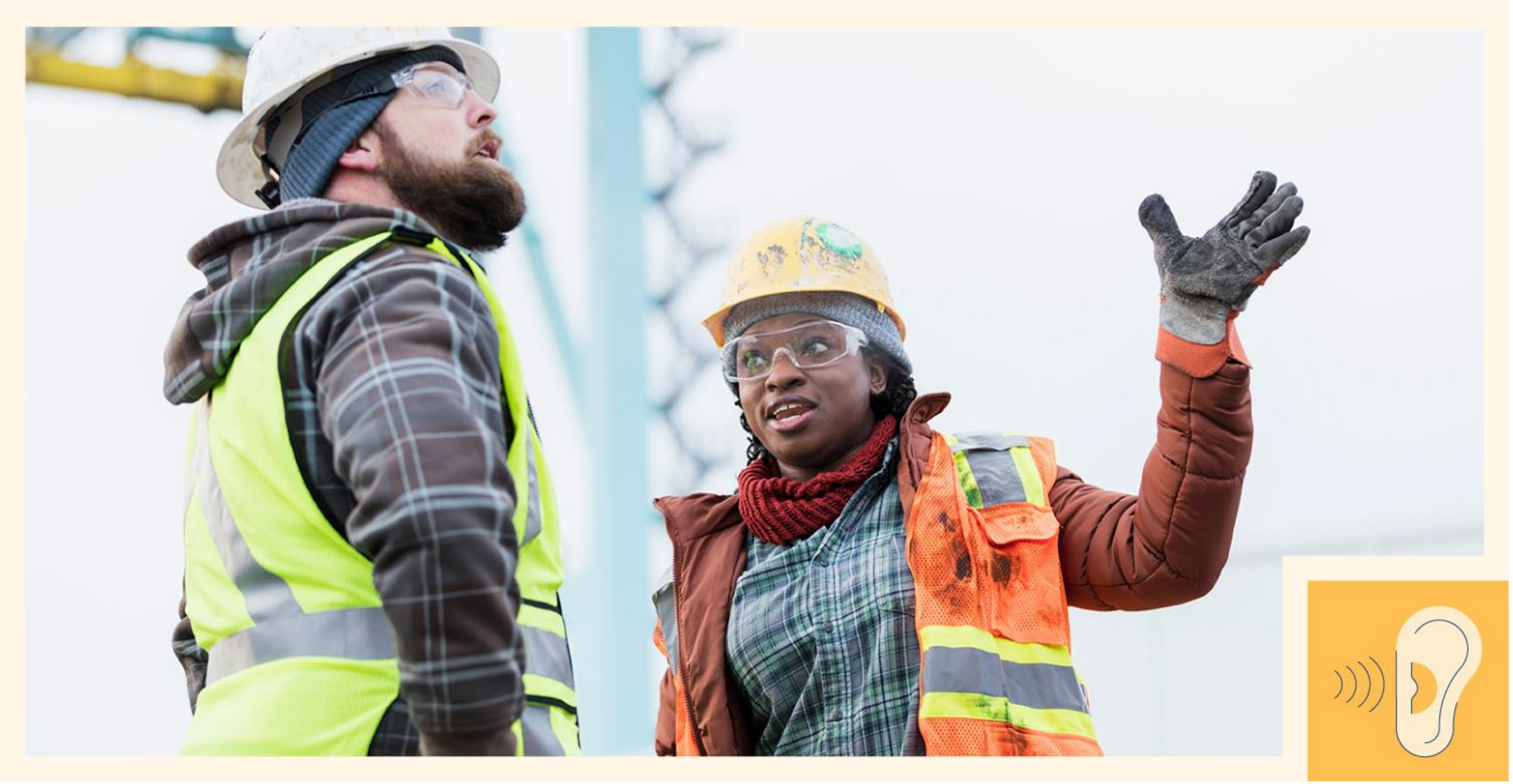

Outline

- Two recent SSI research projects on topics for which geotechnical engineers generally ignore SSI, but including it is important:
  1. Seismic earth pressures acting on flexible vertical retaining walls
  2. Influence of shallow foundations on earthquake-induced ground failure potential

Collaborators

Jonathan Stewart
UCLA

Jason Buenker,
Shannon & Wilson

Maria Giovanna Durante
Università della Calabria

George Mylonakis
Khalifa University

Seismic Earth Pressures

Seismic Earth Pressures

- Mononobe-Okabe (M-O) method is most common method utilized today.
- Begin with static earth pressure (e.g., K_a or K_o). Resultant P_A.
- Limit equilibrium analysis with seismic coefficient k_h ($\propto$ PGA) in Coulomb-type wedge. Produces P_E.
- Predicts very high earth pressures when shaking is strong.
- Empirical evidence is that retaining walls perform well during earthquakes, even if they were not seismically designed.
- Questions:
  - Does horizontal acceleration necessarily give rise to seismic earth pressure?
  - Is seismic earth pressure influenced by factors not considered in M-O method?

$$K_E = \frac{\cos^2(\phi-\eta-\theta)}{\cos\eta\cos^2\theta\cos(\delta+\theta+\eta)\left[1+\sqrt{\frac{\sin(\phi+\delta)\sin(\phi-\eta-\beta)}{\cos(\delta+\theta+\eta)\cos(\beta-\theta)}}\right]^2}$$

$$P_E = \frac{K_E\gamma H^2}{2}$$

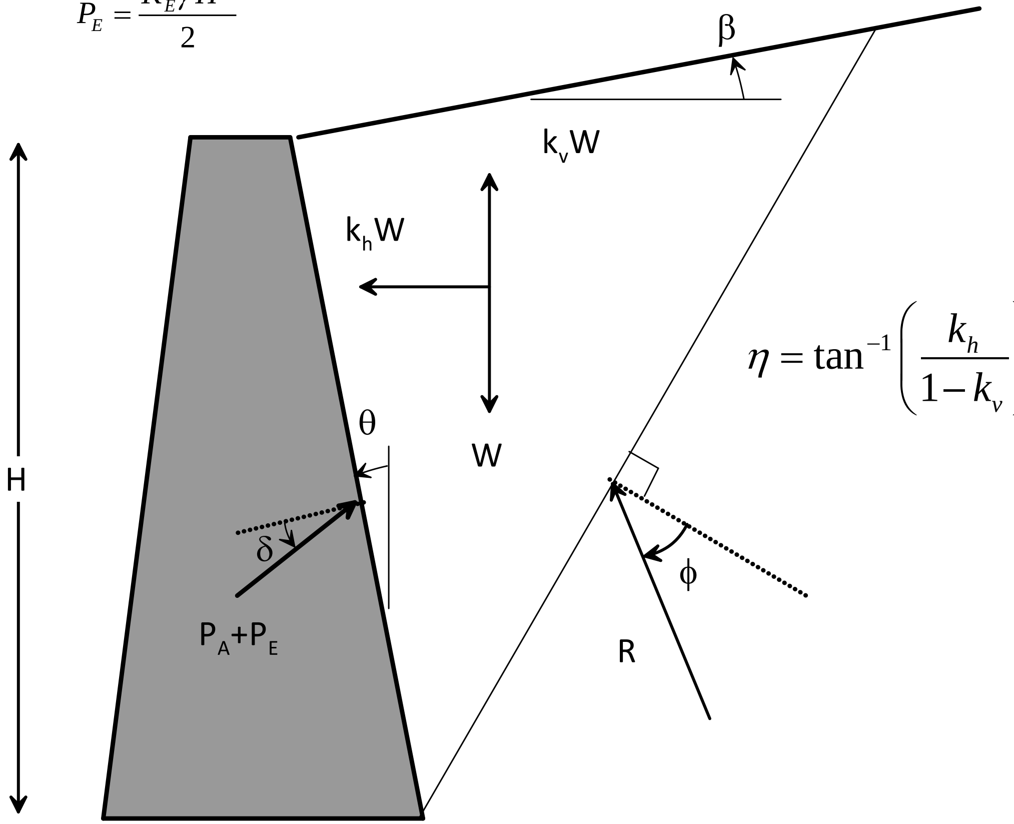

$$\eta = \tan^{-1}\left(\frac{k_h}{1-k_v}\right)$$

Okabe (1924) and **Mononobe and Matsuo (1929)**.

Seismic Earth Pressures

Consider case of vertically propagating, horizontally coherent, SH wave

Acceleration: $\ddot{u}_g(z) = -\omega^2 u_{g0} \cos\left(\frac{\omega z}{V_S}\right) e^{i\omega t}$

Inertia generated by wave resisted by mobilized shear stresses, $\tau_{hv}(z)$

Wave produces no change in normal stresses on vertical or horizontal planes (absent soil plasticity)

If we were to make an excavation and replace the excavated soil with a structural system with the exact same mass and stiffness as the excavated soil, seismic earth pressures would be zero

$\therefore$ Horizontal stresses have no fundamental association with acceleration. Rather, it is relative displacement between the soil and wall that creates earth pressure.

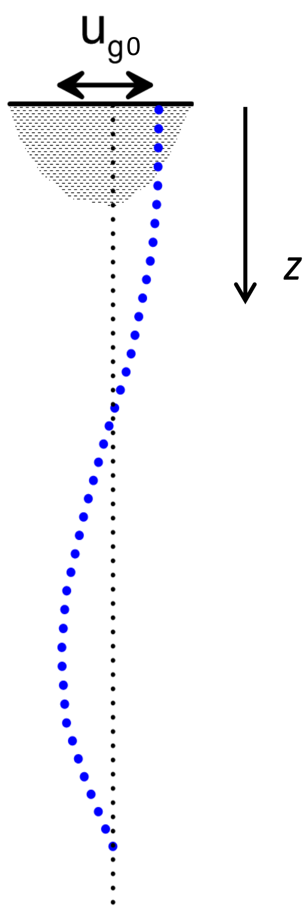

Seismic Earth Pressures

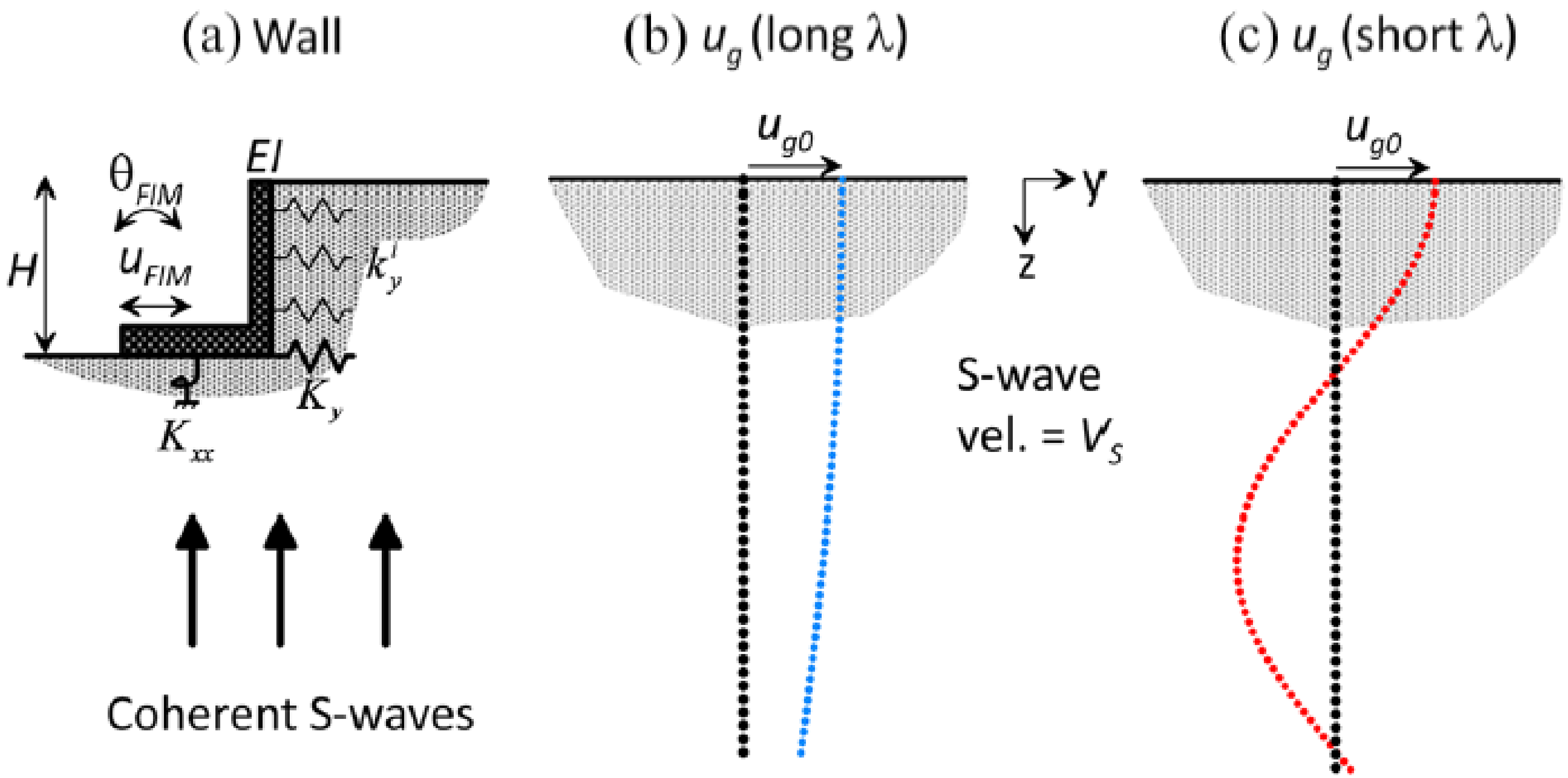

Figure 2. Schematic illustration of free-standing retaining wall subjected to seismic waves with different wavelengths (a) wall, (b) u_g (long λ), and (c) u_g (short λ).

Durante et al. (2022), BSSC (2020).

Seismic Earth Pressures

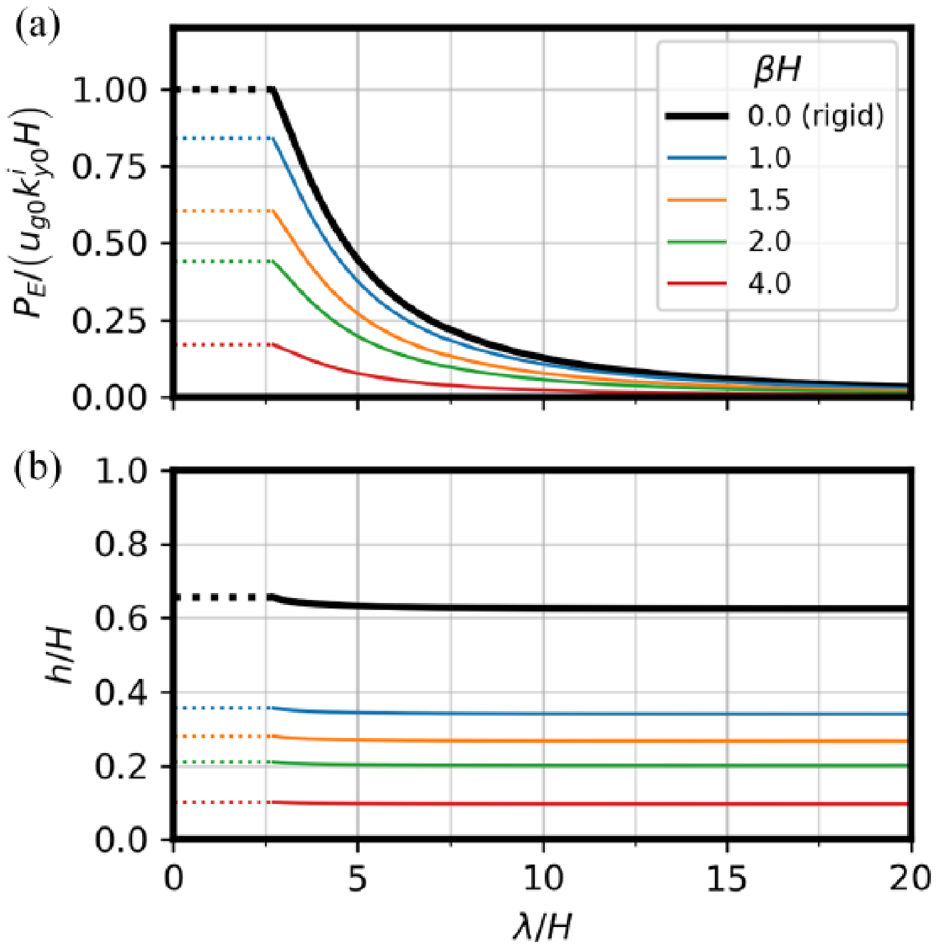

Figure 3. Variation with normalized wavelength λ/H of (a) normalized amplitude of P_E and (b) its point of application above the wall base for various values of βH. Dotted lines at low λ/H are approximations of exact solution.

$$EI\frac{\partial^4 u_w}{\partial z^4} + k_y^i\left[u_{g0}\cos(kz) - u_w\right] = 0$$

$$\beta = \sqrt[4]{\frac{k_y^i}{4EI}}$$

$$u_{g0} = f_u PGV/\omega_m$$

$$f_u = \begin{cases} 0.65 & \text{if } \lambda/H < 2.5 \\ 0.95 & \text{if } \lambda/H > 20 \\ 0.607 + 0.017\lambda/H & \text{otherwise} \end{cases}$$

$$\frac{P_E}{P_{E,rigid}} = \xi = \begin{cases} 1 - \exp\left(1 - \frac{2.9}{\beta H}\right) & \beta H < 1 \\ \sin\left(-0.45 + \frac{1.43}{\beta H}\right) + \cos\left(1.22 + \frac{0.34}{\beta H}\right) & \beta H \geqslant 1 \end{cases}$$

$$\frac{h}{H} = \begin{cases} 0.6 - \exp\left(-0.12 - \frac{2.8}{\beta H}\right) & \beta H < 1 \\ \sin\left(1.68 + \frac{1.5}{\beta H}\right) + \cos\left(2.87 - \frac{1.92}{\beta H}\right) & \beta H \geqslant 1 \end{cases}$$

Durante et al. (2022), BSSC (2020).

Seismic Earth Pressures

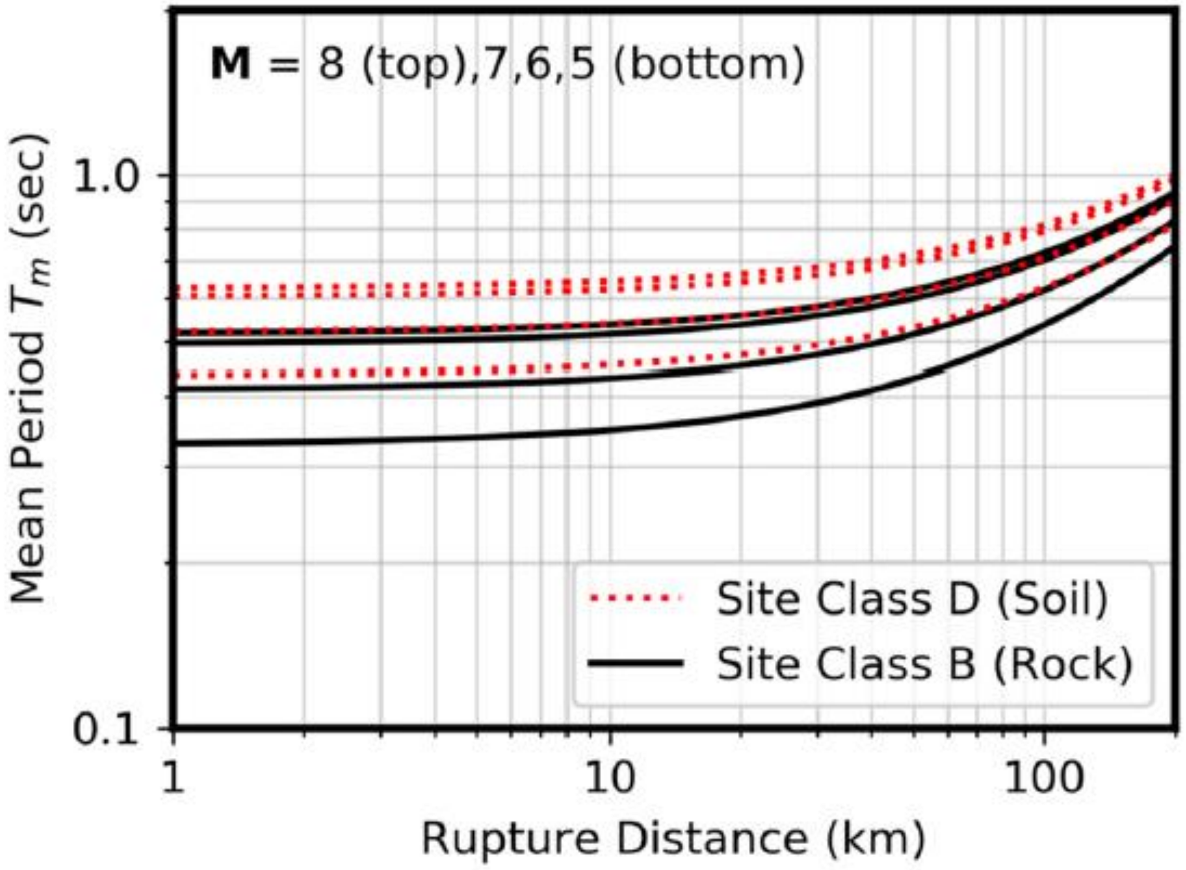

Figure 4. Variation of median values of mean period (T_m) with magnitude, distance, and site condition (Rathje et al., 2004).

Durante et al. (2022), BSSC (2020)

Seismic Earth Pressures

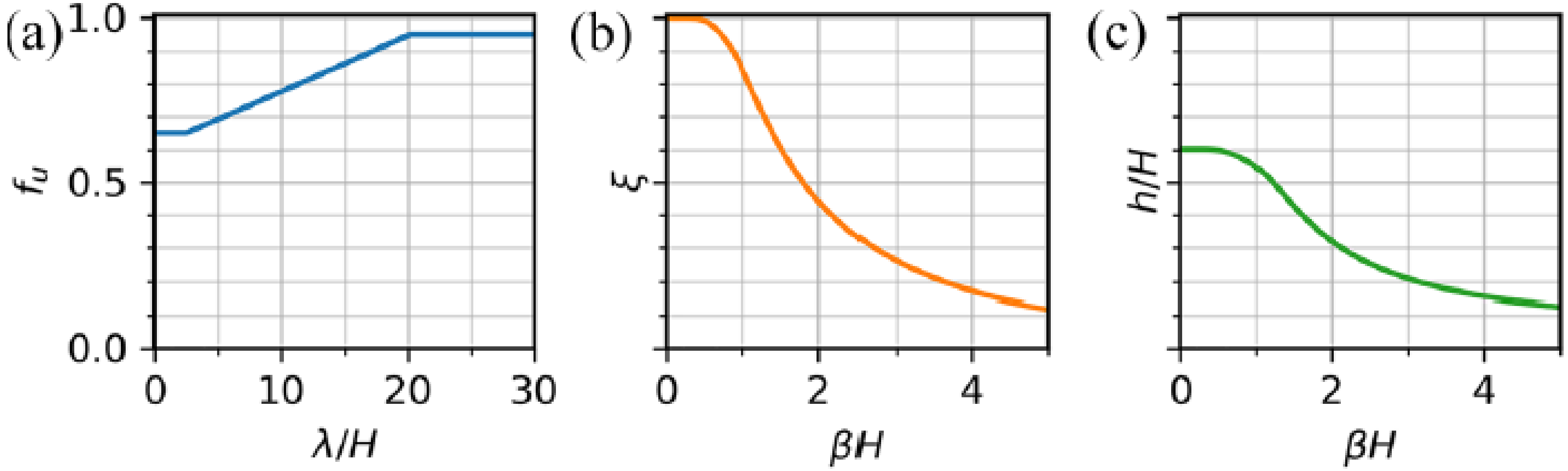

Figure 5. Ground motion amplitude adjustment factor for use with simplified method for evaluation of amplitude of seismic earth pressure resultant force, P_E.

Durante et al. (2022), BSSC (2020)

Seismic Earth Pressures

DESIGNSAFE

Log in | Register

Workspace | Learning Center | NHERI Facilities | NHERI Community | News | Help

Search DesignSafe

DATA DEPOT

Add

Published

Published (NEES)

Community Data

Help

Rename | Move | Copy | Preview | Preview Images | Download | Move to Trash

NEES-2010-0943: SEISMIC EARTH PRESSURES ON RETAINING STRUCTURES

PIs	Nicholas Sitar	**Organizations**	University of California, Berkeley CA, United States
NEES ID	NEES-2010-0943	**Sponsor**	NSF-0936376
Project Type	NEES	**Start Date**	2009-08-01T00:00:00
DOIs	View All DOIs		

Description

Seismic Earth Pressures

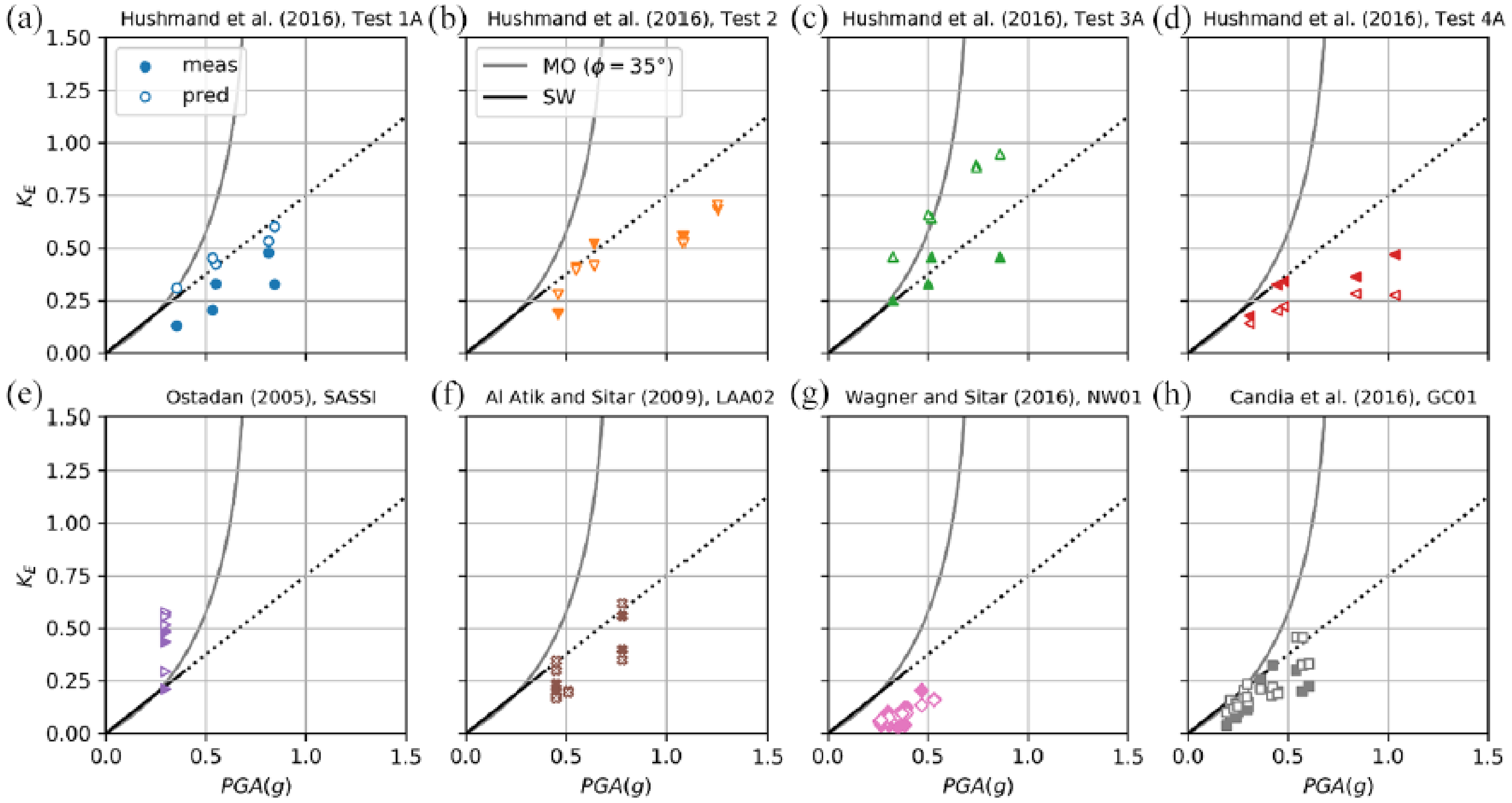

Figure 6. Measured and predicted earth pressure coefficients, K_E, versus *PGA*. The "predicted" values are from the single-frequency simplified procedure presented in this article. (a) Hushmand et al. (2016), Test 1A; (b) Hushmand et al. (2016), Test 2; (c) Hushmand et al. (2016), Test 3A; (d) Hushmand et al. (2016), Test 4A; (e) Ostadan (2005) SASSI analyses; (f) Al Atik and Sitar (2009), Test LAA02; (g) Wagner and Sitar (2016), test NW01; and (h) Candia et al. (2016), test GC01.

Durante et al. (2022).

Seismic Earth Pressures

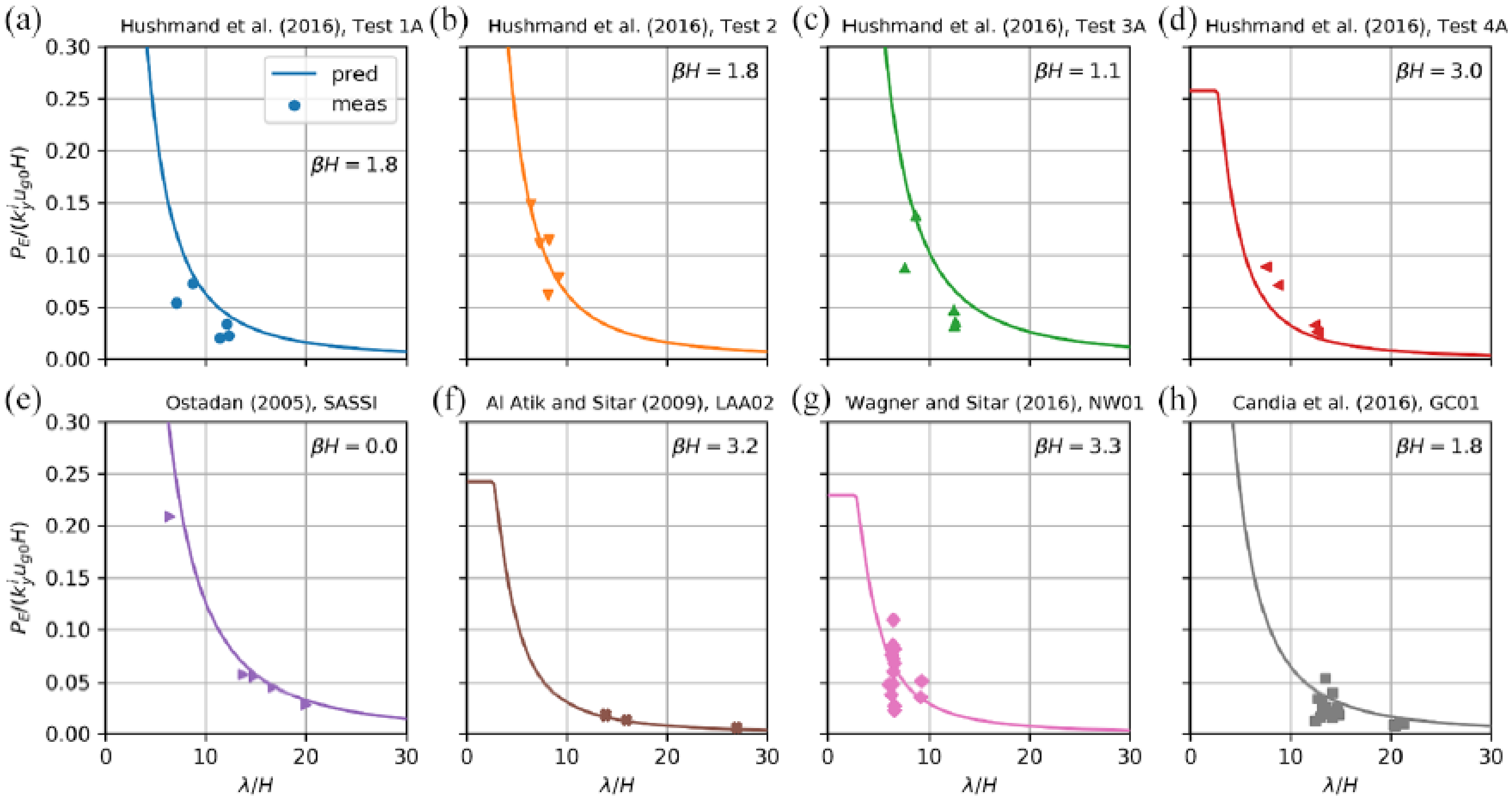

Figure 7. Dimensionless earth pressure, $P_E/\left(k_y^i u_{g0} H\right)$, versus wavelength-to-height ratio, λ/H (a) Hushmand et al. (2016), Test 1A; (b) Hushmand et al. (2016), Test 2; (c) Hushmand et al. (2016), Test 3A; (d) Hushmand et al. (2016), Test 4A; (e) Ostadan (2005), SASSI analyses; (f) Al Atik and Sitar (2009), Test LAA02; (g) Wagner and Sitar (2016), Test NW01; and (h) Candia et al. (2016), Test GC01.

Durante et al. (2022).

Seismic Earth Pressures

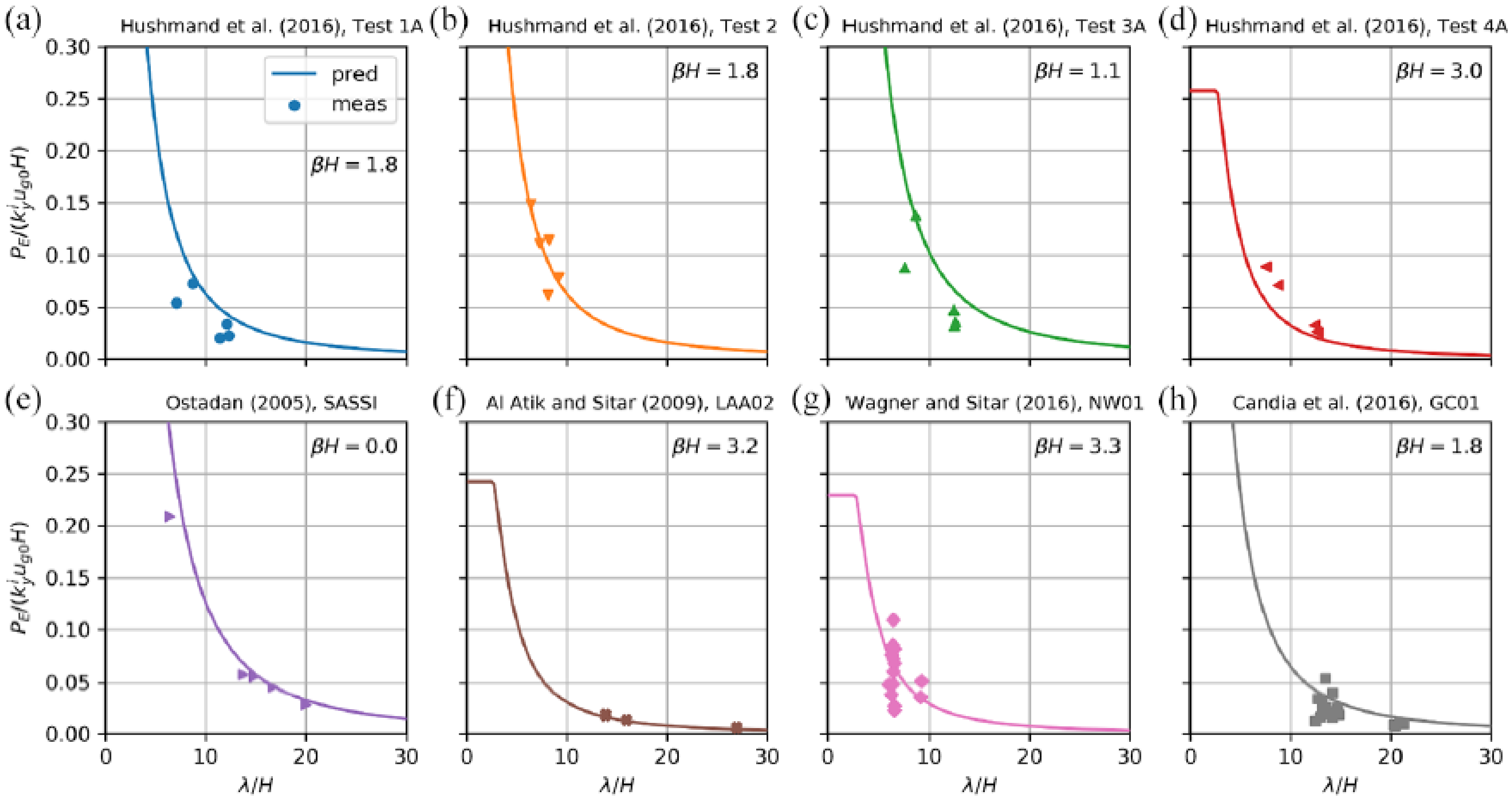

Figure 7. Dimensionless earth pressure, $P_E/\left(k_y^i u_{g0} H\right)$, versus wavelength-to-height ratio, λ/H (a) Hushmand et al. (2016), Test 1A; (b) Hushmand et al. (2016), Test 2; (c) Hushmand et al. (2016), Test 3A; (d) Hushmand et al. (2016), Test 4A; (e) Ostadan (2005), SASSI analyses; (f) Al Atik and Sitar (2009), Test LAA02; (g) Wagner and Sitar (2016), Test NW01; and (h) Candia et al. (2016), Test GC01.

Durante et al. (2022).

Ground Failure

Free-Field Level Ground

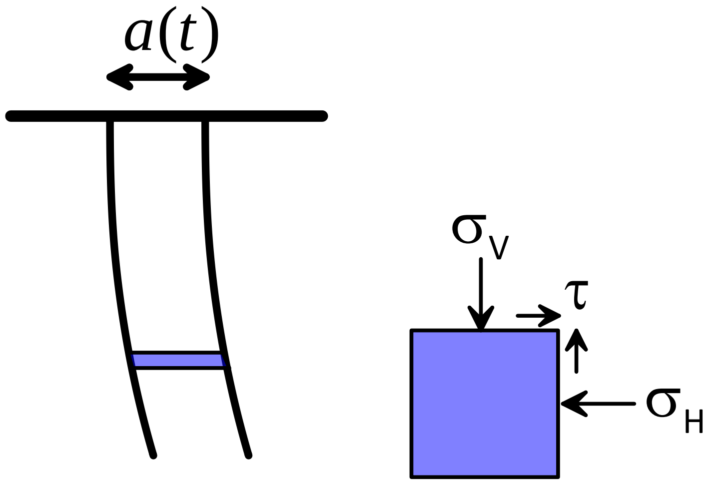

Cyclic Stress Ratio

$$CSR = r_e \cdot \frac{a_{\max}}{g} \frac{\sigma_{vo}}{\sigma_{vo}'} \cdot r_d = 0.65 \cdot \tau_{\max}$$

Cauchy Stress Tensor

$$\underbrace{\begin{bmatrix} \sigma_V & 0 & 0 \\ 0 & \sigma_H & 0 \\ 0 & 0 & \sigma_H \end{bmatrix}}_{\boldsymbol{\sigma}_o} + \underbrace{\begin{bmatrix} 0 & \tau & 0 \\ \tau & 0 & 0 \\ 0 & 0 & 0 \end{bmatrix}}_{\Delta\boldsymbol{\sigma}} = \underbrace{\begin{bmatrix} \sigma_V & \tau & 0 \\ \tau & \sigma_H & 0 \\ 0 & 0 & \sigma_H \end{bmatrix}}_{\boldsymbol{\sigma}}$$

FIGURE 11. View of a 10- to 15-m diameter sand boil deposit about 100 m east of Kornbloom Road (Site 15); this is one of the largest sand boils that erupted during the 1981 event. (Photograph by John Sarmiento.)

Brandenberg et al. (2022)

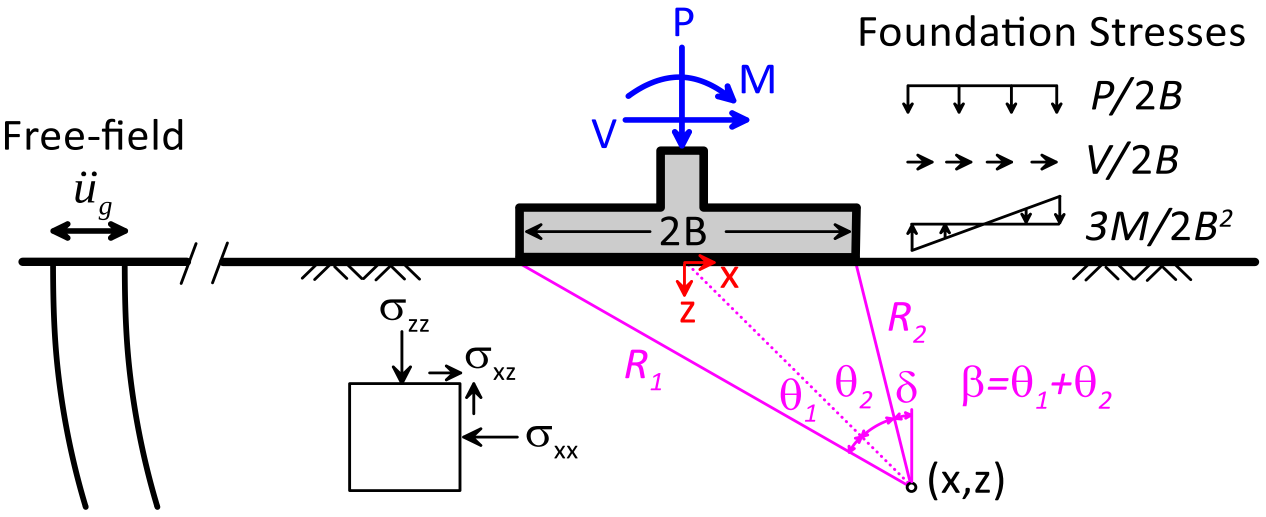

Cauchy Stress Tensor

$$\underbrace{\begin{bmatrix} \sigma_{xx,o} & \sigma_{xy,o} & \sigma_{xz,o} \\ \sigma_{yx,o} & \sigma_{yy,o} & \sigma_{yz,o} \\ \sigma_{zx,o} & \sigma_{zy,o} & \sigma_{zz,o} \end{bmatrix}}_{\boldsymbol{\sigma}_o} + \underbrace{\begin{bmatrix} \Delta\sigma_{xx} & \Delta\sigma_{xy} & \Delta\sigma_{xz} \\ \Delta\sigma_{yx} & \Delta\sigma_{yy} & \Delta\sigma_{yz} \\ \Delta\sigma_{zx} & \Delta\sigma_{zy} & \Delta\sigma_{zz} \end{bmatrix}}_{\Delta\boldsymbol{\sigma}} = \underbrace{\begin{bmatrix} \sigma_{xx} & \sigma_{xy} & \sigma_{xz} \\ \sigma_{yx} & \sigma_{yy} & \sigma_{yz} \\ \sigma_{zx} & \sigma_{zy} & \sigma_{zz} \end{bmatrix}}_{\boldsymbol{\sigma}}$$

Cyclic Stress Ratio

$$CSR = ???$$

Overturning of building B1 as seen from the North-West after the Kocaeli event. (Photo by Jonathan D. Bray)

PEER (2000). Documenting Incidents of Ground Failure Resulting from the August 17, 1999 Kocaeli, Turkey Earthquake. https://apps.peer.berkeley.edu/publications/turkey/adapazari/index.html

SSI Effects on Ground Failure

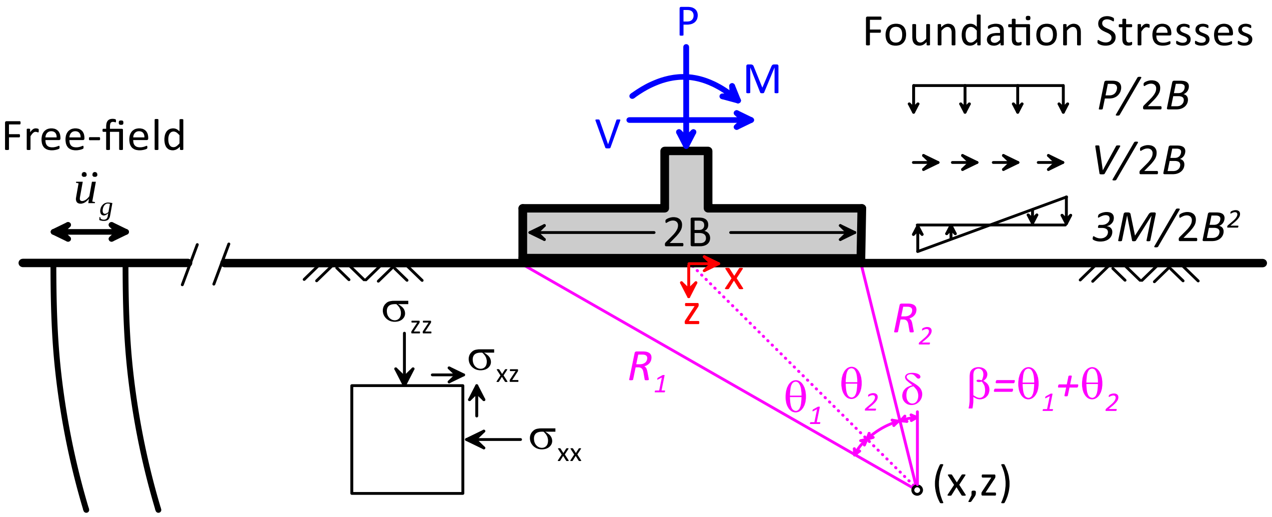

Free-field Stresses

$$\sigma_{zzo,ff} = \rho g z$$

$$\sigma_{xxo,ff} = \sigma_{yyo,ff} = (\rho g z - u) K_o + u$$

$$\Delta\sigma_{xz,ff} = \ddot{u}_g \, \rho \, z \, r_d$$

Assumptions

1. Flexible strip footing
2. Soil is isotropic elastic halfspace
3. Loading frequency is low enough that static solutions are reasonably accurate

SSI Stresses

$$\sigma_{zz,ssi} = \frac{P}{2B\pi}\left[\beta + \sin\beta\cos(\beta+2\delta)\right] + \frac{V}{2B\pi}\left[\sin\beta\sin(\beta+2\delta)\right] + \frac{3M}{4B^2\pi}\left[\frac{2x}{B}\beta - \sin 2\delta - \sin(2\beta+2\delta)\right]$$

$$\sigma_{xx,ssi} = \frac{P}{2B\pi}\left[\beta - \sin\beta\cos(\beta+2\delta)\right] + \frac{V}{2B\pi}\left[\ln\left(R_1^2/R_2^2\right) - \sin\beta\sin(\beta+2\delta)\right] + \frac{3M}{4B^2\pi}\left[\frac{2x}{B}\beta + \frac{2z}{B}\left(\ln\left[R_2^2\right] - \ln\left[R_1^2\right]\right) + \sin 2\delta + \sin(2\beta+2\delta)\right]$$

$$\sigma_{xz,ssi} = \frac{P}{2B\pi}\left[\sin\beta\sin(\beta+2\delta)\right] + \frac{V}{2B\pi}\left[\beta - \sin\beta\cos(\beta+2\delta)\right] + \frac{3M}{4B^2\pi}\left[\cos 2\delta - \cos(2\beta+2\delta) + \frac{2z}{B}(\theta_1 - \theta_2)\right]$$

Brandenberg et al. (2022)

SSI Effects on Ground Failure

$$\begin{Bmatrix} \sigma_1 \\ \sigma_2 \\ \sigma_3 \end{Bmatrix} = eigenvals\left(\begin{bmatrix} \sigma_{xx} & \sigma_{xy} & \sigma_{xz} \\ \sigma_{yx} & \sigma_{yy} & \sigma_{yz} \\ \sigma_{zx} & \sigma_{zy} & \sigma_{zz} \end{bmatrix}\right)$$

Principal stresses

$$q = \sqrt{\frac{1}{2}\left[(\sigma_1 - \sigma_2)^2 + (\sigma_2 - \sigma_3)^2 + (\sigma_1 - \sigma_3)^2\right]}$$

Deviatoric stress invariant

$$p_o' = \frac{\sigma_1' + \sigma_2' + \sigma_3'}{3} = \frac{1}{3} tr(\sigma')$$

Mean effective stress

$$CSR = r_e \frac{\sigma_{vo}}{\sigma_{vo}'} \frac{a_{max}}{g} r_d = r_e \frac{\tau}{\sigma_{vo}'}$$

Classical definition of cyclic stress ratio

Brandenberg et al. (2022)

SSI Effects on Ground Failure

Free-Field Level Ground

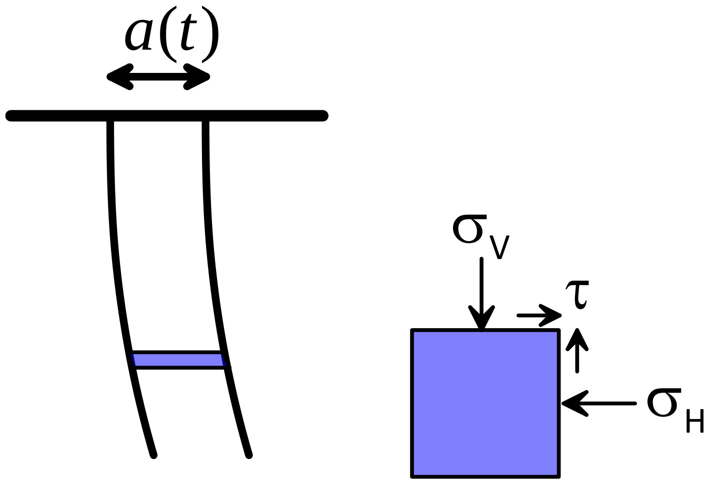

$$CSR = r_e \frac{\sigma_{vo}}{\sigma_{vo}'} \frac{a_{max}}{g} r_d = r_e \frac{\tau}{\sigma_{vo}'}$$

$$\underbrace{\begin{bmatrix} \sigma_V & 0 & 0 \\ 0 & \sigma_H & 0 \\ 0 & 0 & \sigma_H \end{bmatrix}}_{\boldsymbol{\sigma_o}} + \underbrace{\begin{bmatrix} 0 & \tau & 0 \\ \tau & 0 & 0 \\ 0 & 0 & 0 \end{bmatrix}}_{\boldsymbol{\Delta\sigma}} = \underbrace{\begin{bmatrix} \sigma_V & \tau & 0 \\ \tau & \sigma_H & 0 \\ 0 & 0 & \sigma_H \end{bmatrix}}_{\boldsymbol{\sigma}}$$

Invariants

$$p_o' = \sigma_{vo}' \frac{1+2K_o}{3}$$

$$q_o = \sigma_{vo}' - \sigma_{ho}'$$

$$q = \sqrt{q_o^2 + 3\tau^2}$$

$$CSR_q = r_e \frac{1+2K_o}{3p_o'} \sqrt{\frac{\left|q^2 - q_o^2\right|}{3}} sign\left(q - q_o\right)$$

Invariant-based definition of cyclic stress ratio

Brandenberg et al. (2022)

SSI Effects on Ground Failure

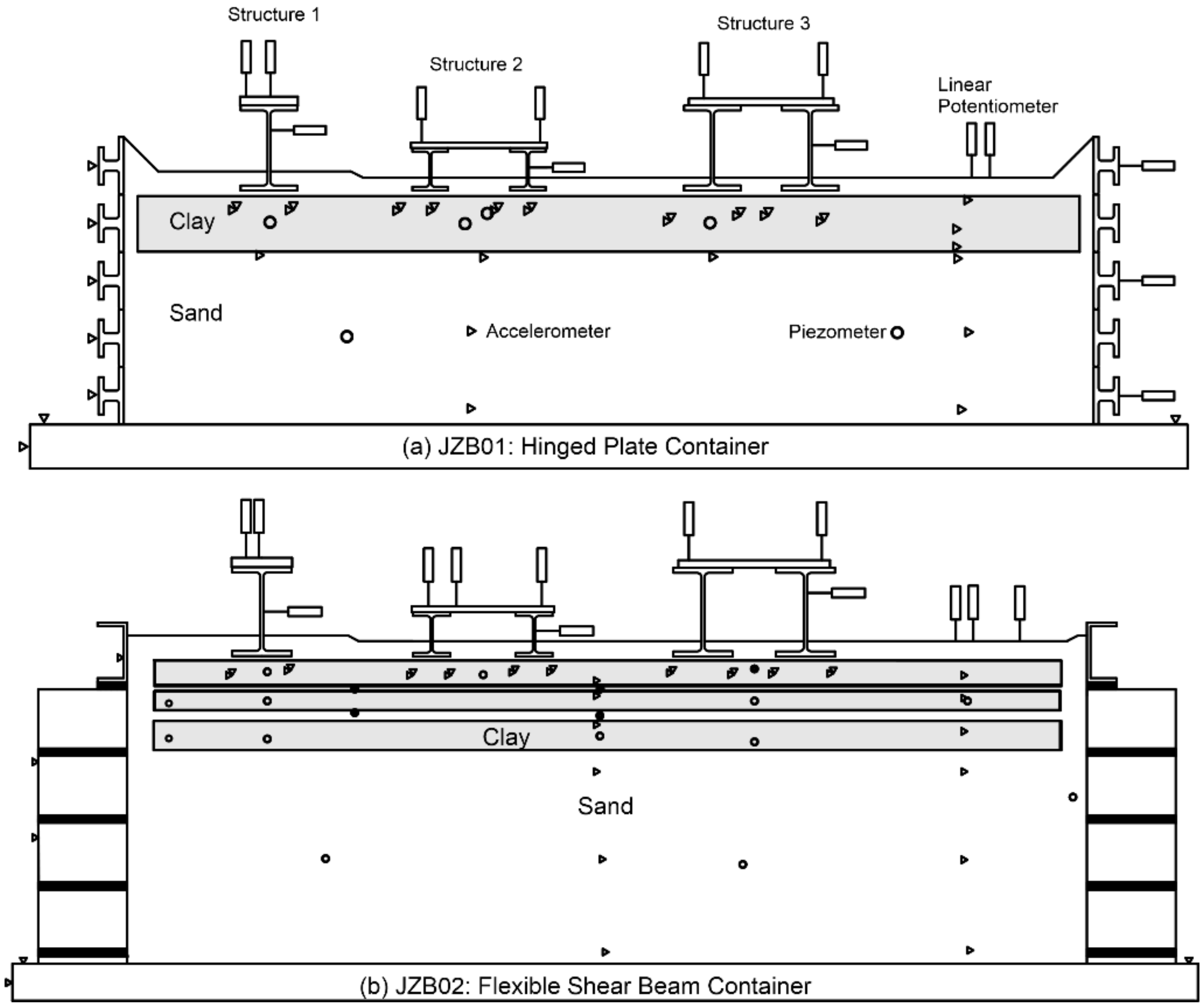

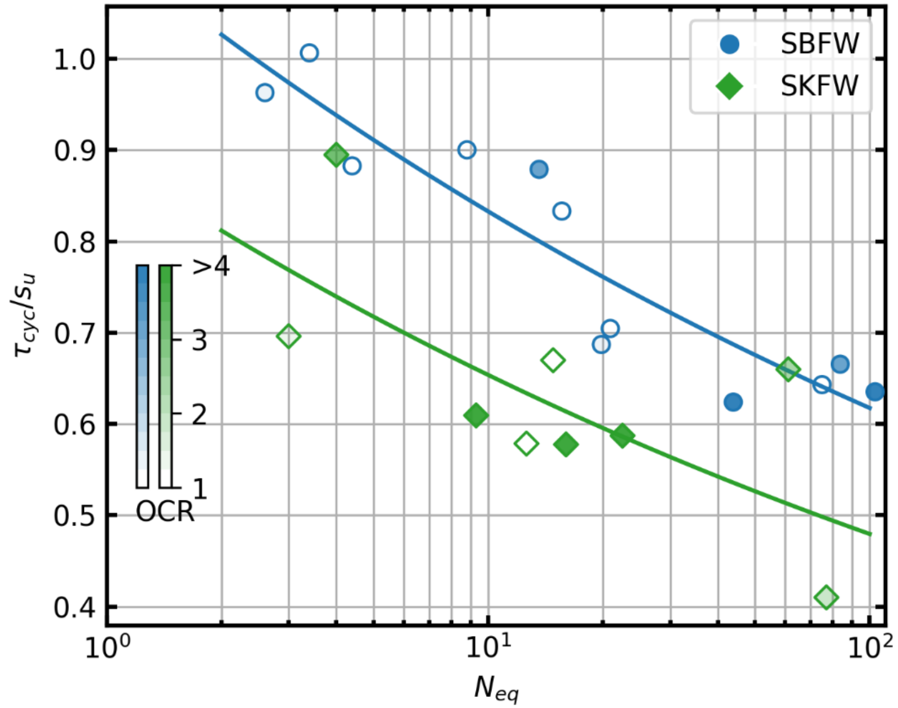

Brandenberg et al. (2022)

SSI Effects on Ground Failure

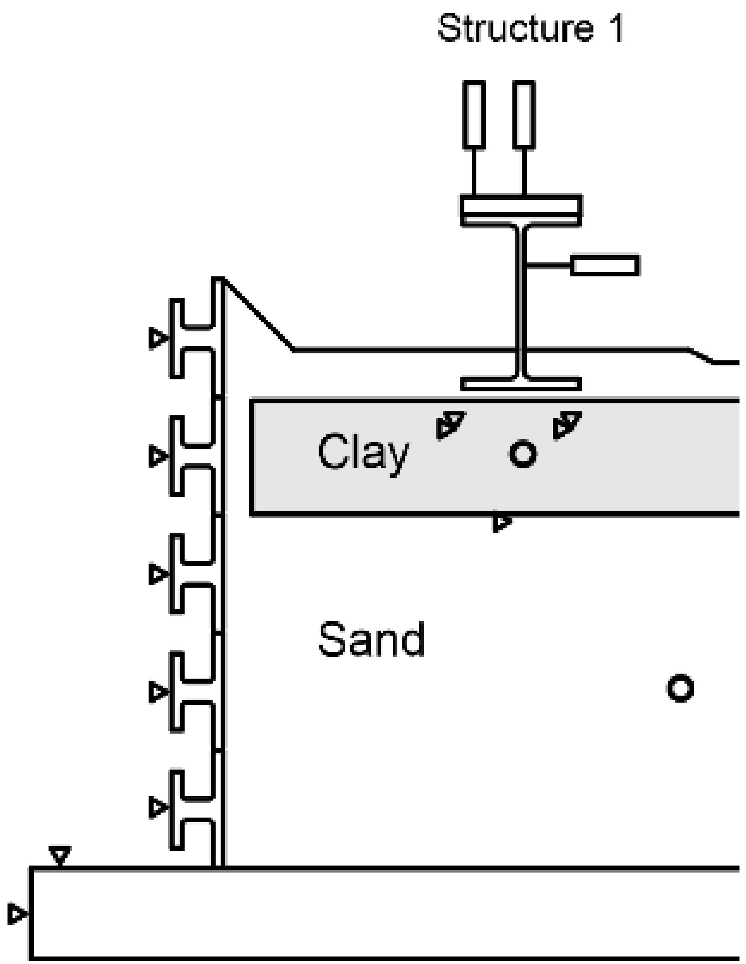

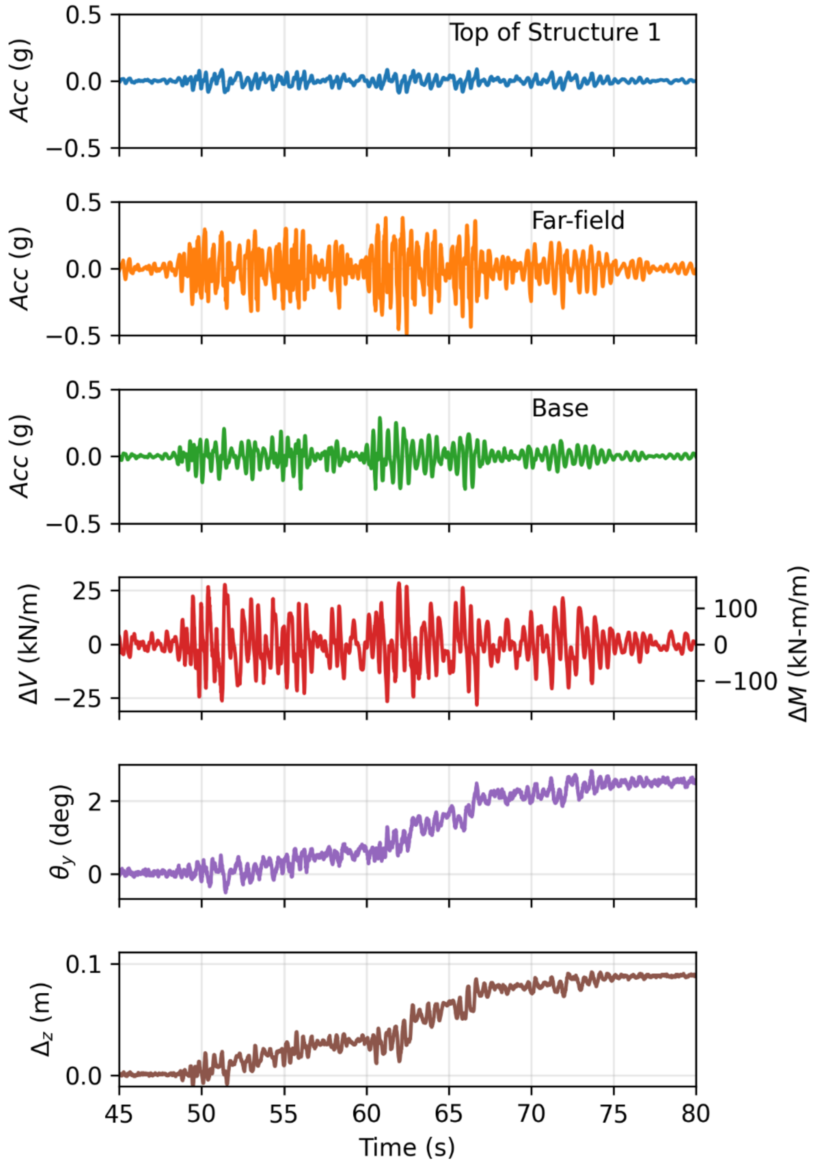

Brandenberg et al. (2022)

SSI Effects on Ground Failure

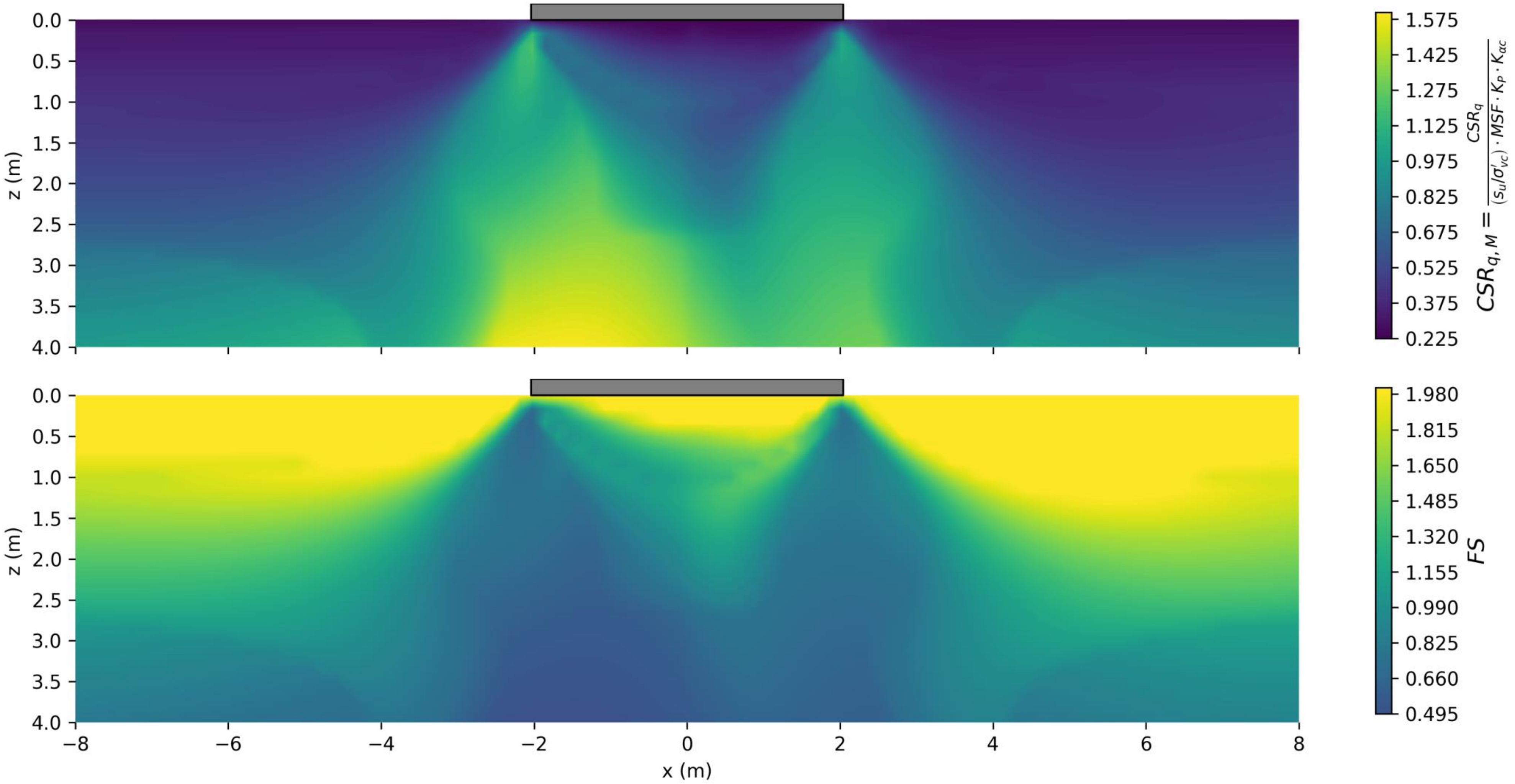

Brandenberg et al. (2022)

SSI Effects on Ground Failure

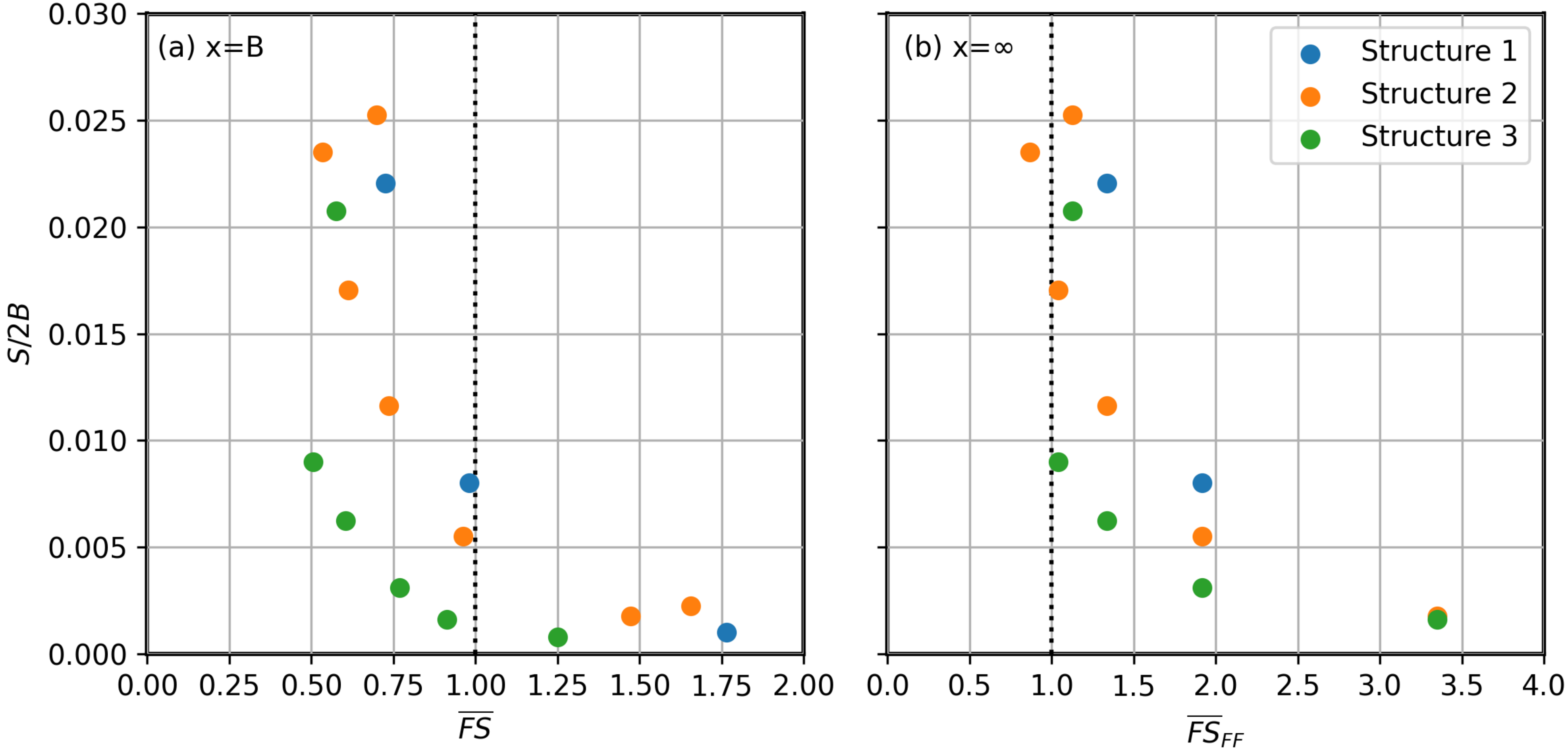

Brandenberg et al. (2022)

Conclusions

- Soil-structure interaction problems are inherently complex because they combine structural and geotechnical disciplines.
- Physical modeling studies provide key insights into fundamental mechanics that allow us to distill the problem into digestible units, and ultimately make design recommendations that are simple and straightforward to implement.
- Publishing experimental data is extremely important to facilitate these insights.

Conclusions

- I presented centrifuge modeling studies today.
- Structural models are necessarily simplified due to centrifuge scaling laws.
- There is tremendous need to validate SSI models using full-scale experiments, like those made possible by the UCSD shake table facility, because we are able to realistically model structural components

Acknowledgments

- **Seismic Earth Pressures:** Partial support for the first author was provided by Caltrans under contract number 65A0413. The first author has recently received funding from the European Union's Horizon 2020 research and innovation programme under the Marie Sklodowska-Curie Grant Agreement number 101029903 – ReStructure 2.0 – H2020 – MSCA – IF – 2020.

- **Ground Failure Potential:** This material is based on work supported by the National Science Foundation under award 1563638. Any opinions, findings, and conclusions or recommendations expressed in this material are those of the authors and do not necessarily reflect the views of the National Science Foundation. Construction of each centrifuge model required extensive help and support provided by the CGM staff and others at UC-Davis. We gratefully acknowledged their assistance. Special thanks to Mandro Eslami for invaluable contributions during the construction and testing of model JZB01 and continued support during model JZB02.

References

Brandenberg, S. J., Buenker, J. M., and Stewart, J. P. (2022) "Evaluation of Ground Failure Potential due to Soil-Structure Interaction and Vertically Propagating Shear Waves." Journal of Geotechnical and Geoenvironmental Engineering, 148(12)

Building Seismic Safety Council (BSSC) (2020) Resource paper 4: Seismic lateral earth pressures. In: NEHRP Recommended Seismic Provisions for New Buildings and Other Structures. Part 3 Resource Papers (Report no. FEMA P-2082, September). Washington, DC: Federal Emergency Management Agency (FEMA), pp. 170–192.

Candia G, Mikola RG and Sitar N (2011) Seismic Earth Pressures on Braced Wall and Displacing Retaining Wall in Clay (GC01). DesignSafe-CI [publisher], doi: 10.4231/D37W67572.

Candia G, Mikola RG and Sitar N (2016) Seismic response of retaining walls with cohesive backfill: Centrifuge model studies. Soil Dynamics and Earthquake Engineering 90: 411–410.

Durant, M.G., Stewart, J.P., Brandenberg, S.J., and Mylonakis, G. (2022). Simplified solution for seismic earth pressures exerted on flexible walls. Earthquake Spectra, 38(3), 1872-1892,

Hushmand A, Dashti S, Davis C and Hushmand B (2016) Seismic performance of underground reservoir structures: Insight from centrifuge modeling on the influence of structure stiffness. Journal of Geotechnical and Geoenvironmental Engineering 142(11): 04016058.

Mononobe N and Matsuo M (1929) On the determination of earth pressure during earthquakes. In: Proceedings of the world engineering congress, Tokyo, Japan, 29 October–7 November.

Okabe S (1924) General theory on earth pressure and seismic stability of retaining wall and dam. Journal of the Japanese Society of Civil Engineering 12(4): 34–41.

Ostadan F (2005) Seismic soil pressure for building walls—An updated approach. Soil Dynamics and Earthquake Engineering 25(7–10): 785–793.

Rathje EM, Dawson C, Padgett JE, Pinelli JP, Stanzione D, Adair A, Arduino P, Brandenberg SJ, Cockerill T, Dey C, Esteva M, Haan FL, Hanlon M, Kareem A, Lowes L, Mock S and Mosqueda G (2017) DesignSafe: New cyberinfrastructure for natural hazards engineering. Natural Hazards Review 18(3): 06017001.

Wagner N and Sitar N (2013) Seismic earth pressures in a deep basement wall on dry sand (NW01). DesignSafe-CI. [publisher], doi: 10.4231/D3D21RJ44